Disorder-enhanced layer Hall effect in a magnetic sandwich heterostructure

Xiao-Xia Yi,[1] Chun-Bo Hua,[2] Rui Chen,[1,*] and Bin Zhou[1,3,†]

[1]*Department of Physics, Hubei University, Wuhan 430062, China*

[2]*School of Electronic and Information Engineering, Hubei University of Science and Technology, Xianning 437100, China*

[3]*Key Laboratory of Intelligent Sensing System and Security of Ministry of Education, Hubei University, Wuhan 430062, China*

(Received 11 November 2023; accepted 20 February 2024; published 4 March 2024)

The layer Hall effect is a type of Hall effect where electrons on the top and bottom layers deflect in opposite directions. In this paper, we investigate the disorder effects on the layer Hall effect in a magnetic sandwich heterostructure that supports the axion insulator and normal insulator phases. We demonstrate that the layer Hall effect in the axion insulator phase is robust against weak disorder. Most interestingly, we find that the layer Hall effect in the normal insulator phase is significantly enhanced with increasing disorder strength. Theoretically, the disorder-enhanced layer Hall effect at weak disorder is explained by using the Born approximation. Experimentally, we suggest the disorder-enhanced layer Hall effect could be detected by applying a perpendicular electric field.

DOI: 10.1103/PhysRevB.109.115301

I. INTRODUCTION

An electron possesses multiple degrees of freedom, such as charge, spin, and valley. These distinct degrees of freedom lead to different types of Hall effects such as the anomalous [1], spin [2], and valley [3] Hall effects. Moreover, electrons possess spatial degrees of freedom, which leads to another type of Hall effect, the layer Hall effect [4–10]. The layer Hall effect describes the electrons in different layers spontaneously deflect in opposite directions. The layer Hall effect was proposed and experimentally observed in the antiferromagnetic topological insulator $MnBi_2Te_4$ [6]. Later, the layer Hall effect was proposed in various materials, such as $MnSb_2Te_4$ [7,8], valleytronic van der Waals bilayers [9], and multiferroic two-dimensional materials [10].

Previous studies have revealed that the layer Hall effects in the axion insulator are significantly enhanced compared to that in normal insulators [6,7]. This phenomenon is attributed to the nontrivial band topology in the axion insulator, which manifests strong hidden layer-locked Berry curvature and the half-quantized surface anomalous Hall effect [11–13], leading to an enhanced layer Hall effect. This feature offers the possibility to observe the significant layer Hall effect in the antiferromagnetic topological insulator $MnBi_2Te_4$ in recent experiments [6,7].

Disorder plays a crucial role in determining the transport in low-dimensional electronic systems [14–18]. Tremendous efforts have been devoted to investigating the disorder effects on different types of Hall effects, such as the anomalous Hall effect [19,20], valley Hall effect [21,22], spin Hall effect [23,24], and quantum Hall effect [25,26]. Moreover, the disorder-induced topological phase, also termed the topological Anderson insulator (TAI), was proposed by Li *et al.* [27]. Later, disorder-induced topological effects were proposed in various systems [28]. Furthermore, the TAI phase had been observed experimentally in one-dimensional disordered atomic wires [29], photonic platforms [30–32], a quantum simulator on a superconducting-circuit device [33], and acoustic systems [34]. However, a systematic study of disorder effects on the layer Hall effect is still absent.

In this paper, we study the disorder effects on the layer Hall effect in a sandwich heterostructure of a magnetically doped system. Depending on the parameter, we find that the system supports the normal insulator and the axion insulator phases. We demonstrate the layer Hall effect is robust against weak disorder in the axion insulator phase. Remarkably, we reveal that the layer Hall effect in the normal insulator phase can be significantly enhanced by increasing the disorder strength. The disorder-enhanced layer Hall effect is explained by using the Born approximation. Finally, we propose that the disorder-enhanced layer Hall effect can be measured by using an external electric field.

This paper is organized as follows. In Sec. II A, we present the Hamiltonian that supports the normal insulator and axion insulator phases. Then, we adopt the layer Hall conductance to characterize the layer Hall effect in Sec. II B. The disorder effects on the layer Hall effect are numerically studied in Sec. III A. In Sec. III B, the disorder-enhanced layer Hall effect is theoretically explained by the Born approximation. In Sec. III C, we propose that the layer Hall effect can be experimentally detected by using a perpendicular electric field. Lastly, a brief discussion and summary are presented in Sec. IV.

II. MODEL AND METHOD

A. Model

To conduct numerical investigations on the layer Hall effect, we use the following four-band tight-binding

*chenr@hubu.edu.cn

†binzhou@hubu.edu.cn

Hamiltonian defined on a cubic lattice [35,36]:

$$H = \sum_i c_i^\dagger \mathcal{M}_0 c_i + \sum_{i,\alpha=x,y,z} \left(c_i^\dagger \mathcal{T}_\alpha c_{i+\alpha} + c_{i+\alpha}^\dagger \mathcal{T}_\alpha^\dagger c_i\right), \quad (1)$$

where $\mathcal{T}_\alpha = B\sigma_0\tau_z - i\frac{A}{2}\sigma_\alpha\tau_x$ describe the hopping term between different sites and $\mathcal{M}_0 = (M - 6B)\sigma_0\tau_z + m(z)\sigma_z\tau_0$. $m(z)$ denotes the magnitude of the magnetization introduced in the z layer, which acts as an effective Zeeman field. The lattice constant is taken to be unity. B and A are model parameters. In the following calculations, we fix the parameters as $A = 0.5$ and $B = 0.25$. σ and τ are Pauli matrices representing spin and orbital, respectively. M determines the Dirac mass of the system.

In our numerical calculations, we adopt the layer Hall conductance $\sigma_{xy}(z)$ to characterize the layer Hall effect (see Appendix A). We take $m(z) = m_z$ for $z = 1, 2$, $m(z) = -m_z$ for $z = n_z - 1, n_z$, and $m(z) = 0$ elsewhere. The system breaks the inversion symmetry $\mathcal{P}$ and time-reversal symmetry $\mathcal{T}$ symmetries but preserves the global space-time $\mathcal{PT}$ symmetry (see Appendix B), which guarantees that the total Hall current is zero [37].

Next, we show that the value of M plays a significant role in determining the topological nature of the system as well as the strength of the layer Hall effect. First, let us consider an infinite sample and neglect the magnetization effects. The topology nature of the system is captured by the axion angle θ [38–40]. When $M < 0$, the system corresponds to a normal insulator phase with $\theta = 0$. When $M > 0$, the system corresponds to a topological insulator with $\theta = \pi$.

Now, we consider a thick-enough film. The topological insulator phase hosts gapless surface Dirac cones on the top and bottom surfaces inside the insulating gap [41]. When local time-reversal symmetry is broken on a certain surface (e.g., through magnetic doping), the gapless surface Dirac state will open a gap, allowing for a half-quantized surface Hall conductance [42]. Moreover, it is noted that the sign of the half-quantized surface Hall conductance depends on the surface magnetization alignment.

As shown in Fig. 1(a), we introduce the magnetization with opposite alignments on the top and bottom surface layers. For a topological insulator, each of the top and bottom surfaces with antiparallel magnetization alignment can host a half-quantized Hall conductance, but with opposite signs, which establishes the axion insulator phase. Recently, the axion insulator phase has attracted much attention because it possesses a unique electromagnetic response from the massive Dirac surface states, giving rise to unique phenomena such as a quantized topological magnetoelectric effect [38–45].

In summary, for a thick-enough axion insulator film, the top and bottom surface layers host Hall current propagating along the opposite directions, which establishes the significant layer Hall effect in the axion insulator phase. Such a signature is absent in a 3D normal insulator, as long as the Fermi energy is located inside the insulating gap.

Moreover, it should be noted that the layer Hall effect is characterized by the hidden layer Berry curvature [6,7]. A system with nonvanishing layer Hall conductance does not indicate the existence of the layer Hall current. In our opinion, it indicates the existence of the hidden layer Hall current that can be revealed by $\mathcal{PT}$-symmetry breaking, such as applying a perpendicular electric field. In this sense, a normal insulator is allowed to host a layer Hall effect.

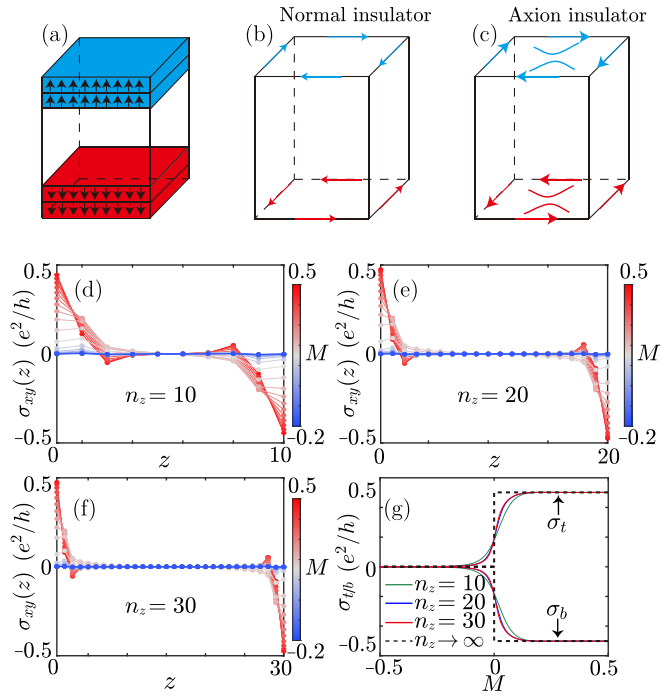

FIG. 1. (a) Schematic illustration of the magnetically doped sandwich structure. Here, we introduce the magnetization with opposite alignments on the top and bottom surface layers. The layer Hall effect in the normal insulator phase shown in (b) is much weaker compared to that in the axion insulator phase shown in (c). (d)–(f) The layer Hall conductance $\sigma_{xy}(z)$ as a function of the layer index z for different M and film thicknesses (d) $n_z = 10$, (e) $n_z = 20$, and (f) $n_z = 30$, respectively. (g) $\sigma_{t/b}$ as functions of the Dirac mass M with different film thickness. Here, $\sigma_{t/b}$ correspond to the Hall conductance of the top and bottom surface layers. In (d)–(g), we take periodic boundary conditions along the x and y directions, and open boundary conditions along the z direction. The Fermi level is 0.01.

B. Layer Hall effect

In the above content, we focus on a thick film. Now, we study the case of a thin film version. It is noted that the quantum confinement has been studied in different kinds of topological insulators, including nonmagnetic topological insulators [46–49] and antiferromagnetic topological insulators [50].

Figures 1(d)–1(f) show the layer Hall conductance $\sigma_{xy}(z)$ as a function of the layer index z, with different film thickness n_z. Here, different colors correspond to different values of the Dirac mass M. It is observed that the layer Hall effect with $M > 0$ is significantly enhanced compared to that with $M < 0$. Such a phenomenon is observed more clearly in Fig. 1(g), where we demonstrate σ_t and σ_b as functions of M. Here $\sigma_t = \sum_{z=1}^{5} \sigma_{xy}(z)$ and $\sigma_b = \sum_{z=n_z-4}^{n_z} \sigma_{xy}(z)$ correspond to the Hall conductance contributed from the top and bottom layers. When M is large enough, the surface Hall conductances reach the half-quantized plateau, with $\sigma_{t/b} = \pm e^2/2h$. As M decreases from 0.5 to -0.5, the surface Hall conductance

gradually decreases and finally diminishes. Moreover, there is a critical point ($M = 0$), which is thickness independent, that separates two size-dependent regions with opposite trends as the film thickness increases. This indicates that in the thermodynamic limit $n_z \to \infty$, the surface Hall conductance is $\pm e^2/2h$ (0) as long as $M > 0$ ($M < 0$) [see the black dashed line in Fig. 1(g)].

In the thermodynamic limit $n_z \to \infty$, as M changes from $M < 0$ to $M > 0$, the system should undergo a topological phase transition from a normal insulator (with no surface Hall conductance) to an axion insulator (with a half-quantized surface Hall conductance). When M changes from $M < 0$ to $M > 0$, the plateau-to-plateau transition shown in Fig. 1(g) is in accordance with the above theoretical predictions. However, for a thin film with a finite thickness n_z, the plateau-to-plateau transitions are destroyed due to the quantum confinement effect. Instead, we observe that the surface Hall conductance evolves from 0 to $\pm e^2/2h$ as M increases. As the thickness increases, the corresponding curve becomes increasingly sharp.

The axion insulators have been confirmed in the antiferromagnetic topological insulators $MnBi_2Te_4$ [51,52] and magnetic topological insulators sandwich structures such as magnetically doped $(Bi,Sb)_2Te_3$ [44,45,53,54]. The layer Hall effect has been studied in previous studies in the antiferromagnetic topological insulator $MnBi_2Te_4$ [6,7]. Our findings regarding the layer Hall effect in the heterostructure of the magnetically doped system are in accordance with the previous studies on $MnBi_2Te_4$.

Moreover, the emergent layer Hall effect with $M < 0$ originates from the crossover from a normal insulator to an axion insulator. This does not indicate that adding magnetization in the top and bottom surfaces of a general normal insulator will render it conductive and accessing its valence/conduction band does not guarantee surface conduction.

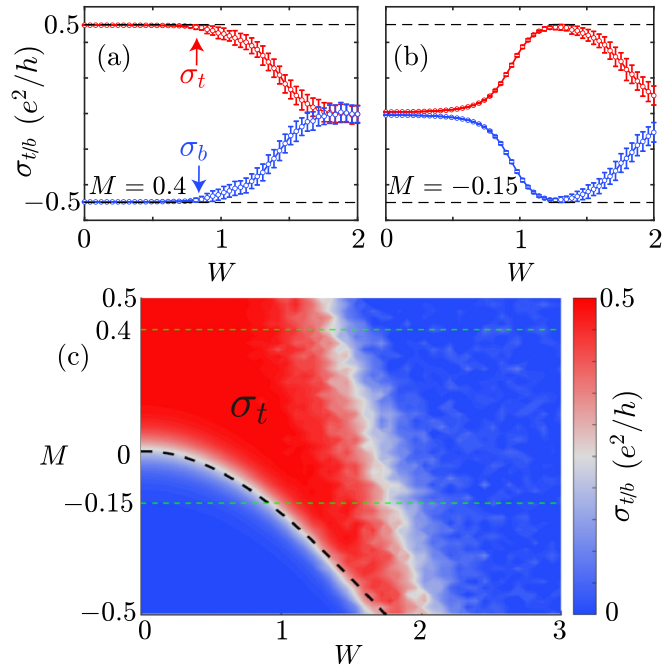

FIG. 2. (a), (b) $\sigma_{t/b}$ as functions of the disorder strength W in (a) the axion insulator phase with the Dirac mass $M = 0.4$ and (b) the normal insulator phase with $M = -0.15$. (c) σ_t as a function of W and M. In (c), the black dashed line corresponds to $\sigma_{t/b} = e^2/4h$, which is obtained by the Born approximation in Eq. (4). In the numerical calculations, we take periodic boundary conditions along the x and y directions and open boundary conditions along the z direction. The system size is taken as $n_x = n_y = 20$ and $n_z = 10$. In (a) and (b), the error bars show the standard deviation of the conductance for 200 samples. In (c), each point is obtained after averaged on 15 independent disorder configurations. The Fermi level is 0.01.

III. DISORDER EFFECT

A. Numerical results

Now we study the disorder effects on the layer Hall effect. We introduce the Anderson disorder to the system with $\Delta H = \sum_i U_i \sigma_0 \tau_0 c_i^\dagger c_i$, where U_i is uniformly distributed within $[-W, W]$, with W being the disorder strength. Figure 2(a) shows the surface Hall conductances $\sigma_{t/b}$ as functions of the disorder strength W for the axion insulator phase with $M = 0.4$. With increasing the disorder strength, the surface Hall conductances keep the half-quantized value until the disorder strength exceeds about $W = 0.9$. Therefore, we show that the layer Hall effect in the axion insulator phase is robust against weak disorder. Further increasing the disorder strength, the half-quantized surface Hall conductance is suppressed by disorder, then gradually decreases and finally collapses to zero.

While for a normal insulator phase with $M = -0.15$ [Fig. 2(b)], in the clean limit, the surface Hall conductance is much smaller compared to that of the axion insulator phase shown in Fig. 2(a). With increasing disorder strength, the disorder-averaged surface Hall conductance first increases, then approaches the half-quantized value with $\sigma_{t/b} = e^2/2h$, and finally decreases. It is noted that the nearly quantization of the disorder-averaged surface Hall conductance is not a coincidence. Such a phenomenon can be explained by the Born approximation explained in the next section, where the disorder is regarded as an effective medium that modifies the value of M.

Figure 2(c) shows the surface Hall conductance σ_t as a function of the disorder strength W and the topological mass M. The disorder-induced topological phase transitions can be demonstrated more clearly. It is observed that the disorder-enhanced layer Hall effect emerges over a broad range of disorder strength. Eventually, for a large disorder strength, the layer Hall effect disappears.

B. Born approximation

The disorder-enhanced layer Hall effect can be explained by using the effective medium theory based on the Born approximation in which high-order scattering processes are neglected [55]. In the Born approximation, the disorder effect is investigated perturbatively and described by the self-energy Σ of the disorder-averaged effective medium

$$(E_F - H_0(\mathbf{k}) - \Sigma)^{-1} = \langle (\tilde{E}_F - \tilde{H}(\mathbf{k}))^{-1} \rangle, \qquad (2)$$

where E_F is the Fermi energy and

$$H_0(\mathbf{k}) = \sum_z c_z^\dagger [M\sigma_0\tau_z + m(z)\sigma_z\tau_0 + 2B(\cos k_x + \cos k_y - 3)\sigma_0\tau_z + A(\sin k_x\sigma_x + \sin k_y\sigma_y)\tau_x]c_z + \sum_z \left(c_z^\dagger \mathcal{T}_z c_{z+1} + c_{z+1}^\dagger \mathcal{T}_z^\dagger c_z\right) \quad (3)$$

is the momentum-space Hamiltonian of the magnetic system with the confinement imposed along the z direction. $\tilde{E}_F$ and $\tilde{H}(\mathbf{k})$ correspond to the renormalized Fermi energy and renormalized Hamiltonian due to the self-energy Σ induced by disorder. The self-energy Σ is expressed through the following integral equation [55]:

$$\Sigma = \frac{W^2}{12\pi^2}\int_{\mathrm{FBZ}} d\mathbf{k}[E_F - H_0(\mathbf{k}) - \Sigma + i\eta]^{-1}, \quad (4)$$

where η is an infinitesimal number. This integration is over the first Brillouin zone (FBZ). We will use the lowest-order Born approximation, which means setting $\Sigma = 0$ on the right-hand side of Eq. (4).

Through numerical calculations, we observe that the self-energy has the following form:

$$\Sigma = \sum_z c_z^\dagger(\Sigma_0\sigma_0\tau_0 + \Sigma_M\sigma_0\tau_z)c_z. \quad (5)$$

It is noted that both the Fermi energy E_F and the self-energy term Σ_0 are expressed in terms of $\sigma_0\tau_0$, and the Dirac mass M and the self-energy term Σ_M are expressed in terms of $\sigma_0\tau_z$. Thus, the Fermi energy E_F and Dirac mass are renormalized by disorder with $\tilde{E}_F = E_F - \Sigma_0$ and $\tilde{M} = M + \Sigma_M$, respectively. By calculating the Hall conductance of the renormalized Hamiltonian $\tilde{H}(\mathbf{k}) = H(\mathbf{k}) + \sum_z c_z^\dagger \Sigma_M\sigma_0\tau_z c_z$, we obtain the black dashed line in Fig. 2(c). The results based on the Born approximation are in agreement with the numerical results. This indicates that the disorder is regarded as an effective medium that modifies the value of M, which give rise to the disorder-enhanced layer Hall effect.

C. Experimental proposal for detecting the disorder-enhanced layer Hall effect

The layer Hall effect in the axion insulator phase has been observed in the antiferromagnetic topological insulator $MnBi_2Te_4$ [6] by measuring the emergent Hall conductance, which is a result of the broken $\mathcal{PT}$ symmetry in the presence of the electric field. Here, we suggest that the disorder-enhanced layer Hall effect can be experimentally detected by applying an external electric field.

Figure 3 shows the Hall conductance $\sigma_{xy} = \sum_{z=1}^{n_z}\sigma_{xy}(z)$ as functions of the Fermi energy E_F for different external electric fields V and disorder strengths W. In the clean limit (i.e., $W = 0$), the electric field induces a nonzero Hall conductance in both the axion and normal insulator phases [Figs. 3(a) and 3(e)]. However, the electric-field-induced Hall conductance exhibits distinct characteristics in the two systems. In the axion insulator, the induced Hall conductance can occur when the Fermi energy resides within the bulk band gap [Fig. 3(a)]. Such a signature is absent in the normal insulator phase, where the induced Hall conductance emerges only when the Fermi energy is near the bulk band edge [Fig. 3(e)]. Furthermore, for a certain Fermi surface, the induced Hall conductance has an opposite sign compared to that in normal insulators.

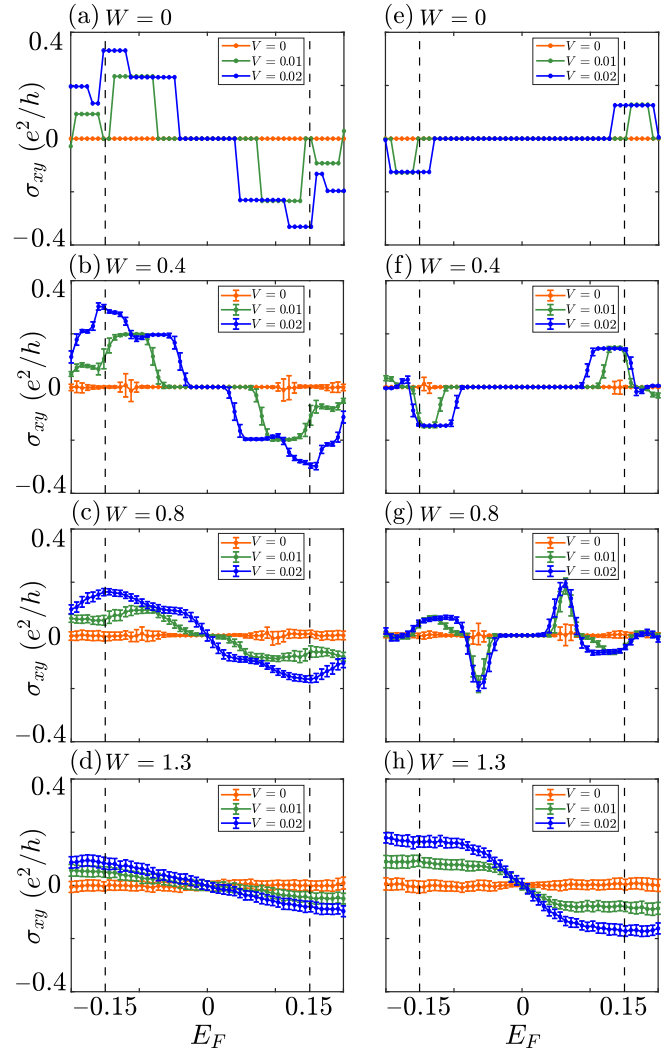

FIG. 3. Hall conductance as functions of the Fermi energy E_F, for different voltages V and disorder strengths W. (a)–(d) Axion insulator phases with Dirac mass $M = 0.15$. (e)–(h) Normal insulator phases with $M = -0.15$. In the numerical calculations, we take periodic boundary conditions along the x and y directions and open boundary condition along the z direction. The system size is $n_x = n_y = 20$ and $n_z = 10$. Here, the area enclosed by the black dashed lines corresponds to the bulk band gap without the electric field and the disorder effect.

The mechanism is explained in Figs. 4(a), 4(e), and Appendix C. In the absence of the electric field, the two systems preserve the $\mathcal{PT}$ symmetry and the energy states are double degenerate. The $\mathcal{PT}$ symmetry guarantees that the Hall conductance of the system is zero. The electric field breaks the $\mathcal{PT}$ symmetry, leading to an energy offset between the degenerate bands and enabling the emergence of the Hall conductance (this is explained more clearly in Appendix C). On the other hand, the axion insulators host surface state inside the bulk gap. Once the electric field is introduced, the compensated nature of the occupied bands is destroyed, which

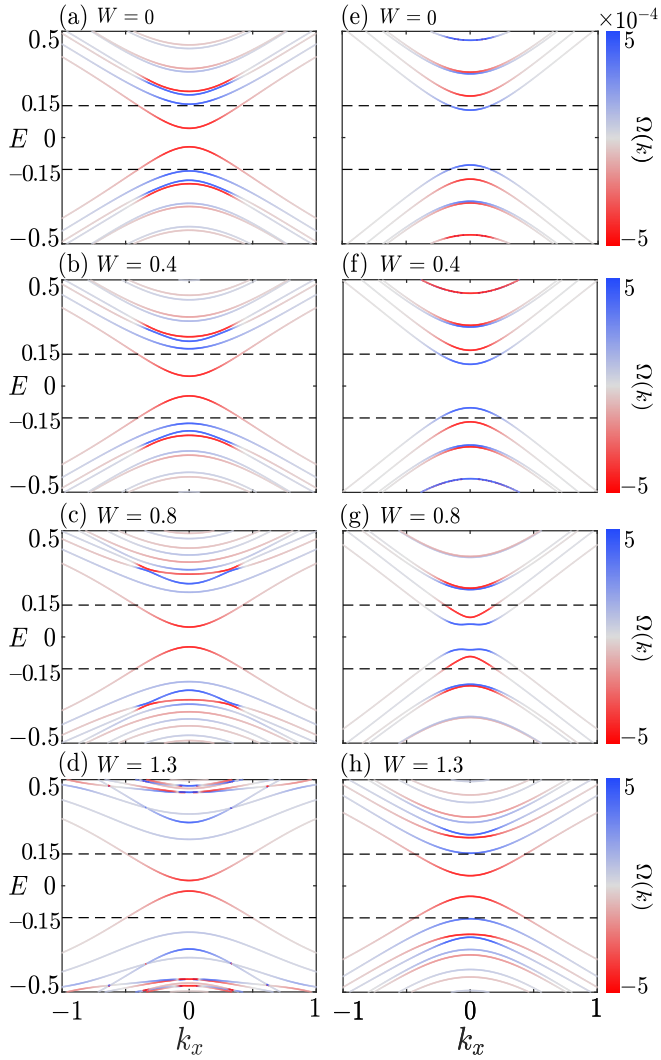

FIG. 4. Energy spectrum as a function of k_x at $k_y = 0$ for different disorder strengths W. Here, the color scheme indicates the Berry curvature distribution. (a)–(d) Axion insulator phases with Dirac mass $M = 0.15$. (e)–(h) Normal insulator phases with $M = -0.15$. The film thickness is taken as $n_z = 10$ and the strength of the voltage is $V = 0.02$. Here, the area enclosed by the black dashed lines corresponds to the bulk band gap without the electric field and the disorder effect. In (b)–(d) and (f)–(h), the spectrum for different disorder strengths is evaluated from the renormalized Hamiltonian $H + \Sigma$ by using the Born approximation in Eq. (4).

results in a nonzero Hall conductance when the Fermi energy crosses the spilt surface states located within the bulk gap [Fig. 4(a)]. However, in the normal insulator, the induced Hall conductance is only observed when the Fermi energy crosses the bulk bands because there is no in-gap state [Fig. 4(e)]. Moreover, since the occupied bands are dominated by opposite Berry curvatures [Figs. 4(a) and 4(e)], the sign of the induced Hall conductance is of opposite signs for the axion and normal insulators for a certain Fermi energy [Figs. 3(a) and 3(e)].

When disorder is introduced, for both the axion and normal insulator phases, the regimes with nonvanishing Hall conductance appear more close to the Dirac point ($E_F = 0$) [Figs. 3(b)–3(d) and Figs. 3(f)–3(h)]. For the axion insulator, the induced Hall conductance collapses with the increasing disorder strength [Figs. 3(b)–3(d)]. We observe distinct phenomena in the normal insulator phase [Figs. 3(f)–3(h)]. For moderate disorder strength [Fig. 3(h)], the induced Hall conductance reverts its sign and becomes more significant compared to the case with weaker disorder strength [Fig. 3(e)].

The disorder-induced phenomenon in Figs. 3(b)–3(d) and Figs. 3(f)–3(h) can be explained by calculating the spectrum of the renormalized Hamiltonian shown in Figs. 4(b)–4(d) and Figs. 4(f)–4(h), respectively. The bulk gap of the renormalized Hamiltonian decreases with increasing disorder strength, which leads to the shift of the regime with nonzero Hall conductance in Figs. 3(b)–3(d) and Figs. 3(f)–3(h). Further increasing the disorder strength, the system crosses over from the normal insulator to the axion insulator, accompanied by the emergence of the gapped surface states inside the bulk gap. Thus, it is the gapped surface states that give rise to the significant electric-field-induced Hall conductance shown in Fig. 3(h). We propose that such signatures may serve as a probe for detecting the disorder-enhanced layer Hall effect in the future.

In addition, the induced Hall conductance exhibits different plateaus in Figs. 3(a) and 3(e). This is due to finite-size effects in the real-space calculations. In Appendix B, we demonstrate that the electric-field-induced Hall conductance, when computed in momentum space, exhibits an analogous behavior to the real-space calculations illustrated in Fig. 3(a), but displays a smoother curve.

IV. CONCLUSION AND DISCUSSION

In this paper, we study the disorder effect on the layer Hall effect. In the axion insulator phase, we show that the layer Hall effect characterized by the half-quantized surface Hall conductance is robust against weak disorder. Most interestingly, in the normal insulator phase, we find that the layer Hall effect is significantly enhanced due to the disorder effect. The mechanism for the disorder-enhanced layer Hall effect is explained by adopting the Born approximation. We also propose that the disorder-enhanced layer Hall effect can be experimentally detected by applying a perpendicular electric field.

Based on our current results, the disorder-enhanced layer Hall effect in the normal insulator phase may only apply in systems that potentially can be turned into an axion phase. In future work, we will continue to investigate whether disorder can enhance the layer Hall effect in a wider range of systems.

ACKNOWLEDGMENTS

R.C. acknowledges the support of the NSFC (under Grant No. 12304195) and the Chutian Scholars Program in Hubei Province. B.Z. was supported by the NSFC (under Grant No. 12074107), the program of outstanding young and middle-aged scientific and technological innovation team of colleges and universities in Hubei Province (under Grant No. T2020001) and the innovation group project of the Natural Science Foundation of Hubei Province of China (under

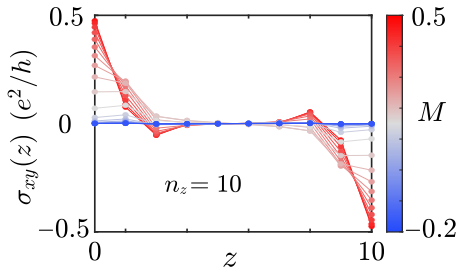

FIG. 5. The layer Hall conductance $\sigma_{xy}(z)$ calculated in real space as a function of the layer index z for different M. In the numerical calculations, we take periodic boundary conditions along the x and y directions and open boundary conditions along the z direction. The system size is taken as $n_x = n_y = 20$ and $n_z = 10$.

Grant No. 2022CFA012). C.-B.H. was supported by the NSFC (Grant No. 12304539) and the Doctoral Research Start-Up Fund of Hubei University of Science and Technology (Grant No. BK202316).

APPENDIX A: LAYER HALL CONDUCTANCE

1. Layer Hall conductance in the momentum space

In the absence of disorder, the system preserves the transitional symmetry and can be characterized by the layer Hall conductance calculated in the momentum space. For the mth occupied band, the layer-resolved Hall conductance in the momentum space is expressed as [56–58]

$$\tilde{\sigma}_m(z) = \frac{e^2}{2\pi h}\int d^2\mathbf{k}\mathcal{F}^{mm}_{xy}(\mathbf{k}, z), \tag{A1}$$

where

$$\mathcal{F}^{mn}_{\alpha\beta}(\mathbf{k}) = \partial_\alpha \mathcal{A}^{mn}_\beta(\mathbf{k}) - \partial_\beta \mathcal{A}^{mn}_\alpha(\mathbf{k}) \tag{A2}$$

$$+ i\left[\mathcal{A}^{mn}_\alpha(\mathbf{k}), \mathcal{A}^{mn}_\beta(\mathbf{k})\right] \tag{A3}$$

is the non-Abelian Berry curvature in terms of $\mathcal{A}^{mn}_\alpha(\mathbf{k}, z)$ with the band indexes m and n. The Hall conductance of all occupied bands of the layer is given by $\tilde{\sigma}(z) = \sum_{E_m<E_F}\tilde{\sigma}_m(z)$, where the Hall conductance of the mth band is $\sigma_m = \sum_{z=1}^{n_z}\tilde{\sigma}_m(z)$.

2. Layer Hall conductance in the real space

In the presence of disorder, the system breaks the transitional symmetry and can be characterized by the layer Hall conductance calculated in the real space. The layer Hall conductance can be calculated by summing up the layer-resolved real-space Berry curvature [59,60],

$$\Omega_z = 2\pi i \mathrm{Tr}\{\hat{P}[-i[\hat{x}, \hat{P}], -i[\hat{y}, \hat{P}]]\}_z, \tag{A4}$$

where we take periodic boundary conditions along the x and y directions and open boundary conditions along the z direction. $\hat{x}$ and $\hat{y}$ are the coordinate operators in the real space. Here, the trace is over the zth level, P is the projection operator performed on the occupied states. In the real space, the Hall conductance of each layer is $\sigma_{xy}(z) = \frac{e^2}{h}\Omega_z$ and the total Hall conductance is given by $\sigma_{xy} = \sum_z \sigma_{xy}(z)$. Figure 5 shows the real-space layer Hall conductance $\sigma_{xy}(z)$ as a function of the layer index z for different values of the Dirac mass M, which is in accordance with that calculated in the momentum space [Fig. 1(d)].

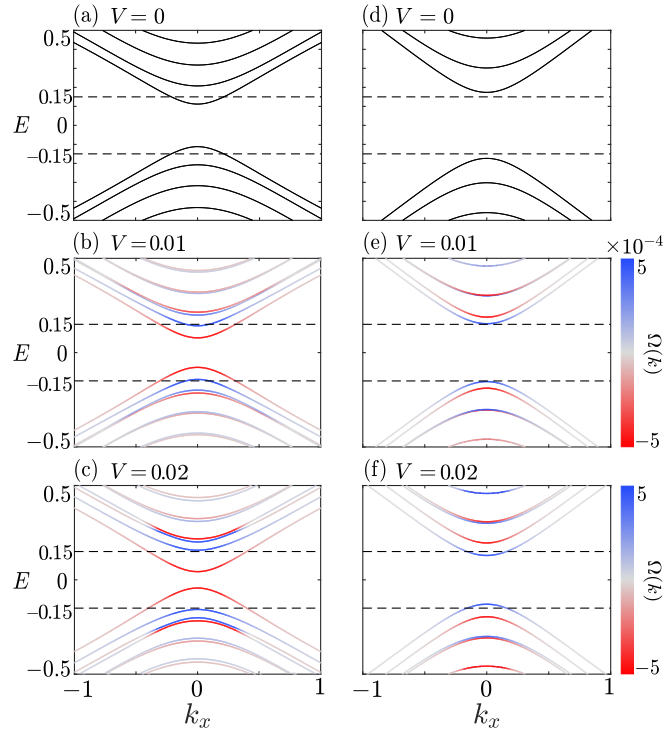

FIG. 6. Energy spectra as a function of k_x at $k_y = 0$ for different voltages V. Here, the color scheme indicates the Berry curvature distribution. (a)–(c) Axion insulator phases with Dirac mass $M = 0.15$. (d)–(f) Normal insulator phases with $M = -0.15$. The film thickness is taken as $n_z = 10$. Here, the area enclosed by the black dashed lines corresponds to the bulk band gap without the electric field and the disorder effect.

APPENDIX B: $\mathcal{PT}$ SYMMETRY

In the absence of magnetization, the system satisfies the following symmetries:

$$\mathcal{T}H(\mathbf{k})\mathcal{T}^{-1} = H(-\mathbf{k}),$$
$$\mathcal{P}H(\mathbf{k})\mathcal{P}^{-1} = H(-\mathbf{k}),$$
$$\mathcal{PT}H(\mathbf{k})(\mathcal{PT})^{-1} = H(\mathbf{k}), \tag{B1}$$

where $\mathcal{T} = I_{nz}\sigma_y\tau_0\mathcal{K}$ is the time-reversal symmetry, I_{nz} is the identity matrix and $\mathcal{K}$ is the complex conjugation. $\mathcal{P} = \mathcal{M}\sigma_0\tau_z$ depicts the inversion symmetry and $\mathcal{M}$ is the orthogonal matrix permuting the layers of the whole system perpendicularly. When the magnetization is included, the system breaks the inversion symmetry $\mathcal{P}$ and the time-reversal symmetry $\mathcal{T}$, but preserves the global space-time $\mathcal{PT}$ symmetry [61,62].

APPENDIX C: LAYER HALL EFFECT IN THE PRESENCE OF THE ELECTRIC FIELD

Here, we present more details of the numerical results on the layer Hall effect. In the absence of the electric field, the axion insulator and the normal insulator preserve the $\mathcal{PT}$ symmetry and the energy states are double degenerate

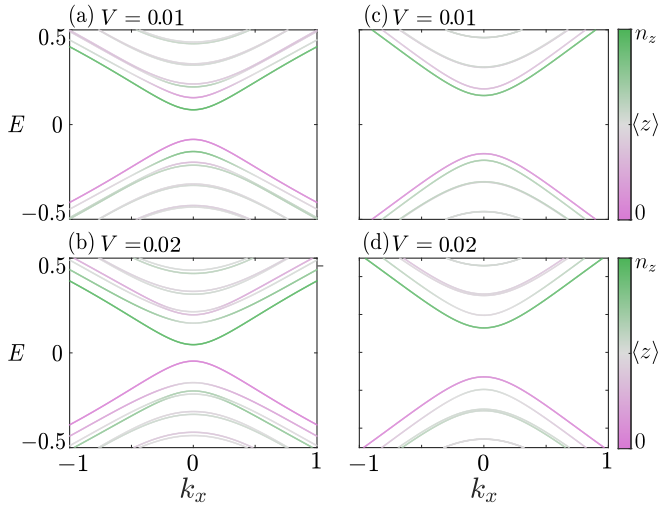

FIG. 7. Energy spectra as a function of k_x at $k_y = 0$ for different voltages V. Here, the color scheme indicates the wave function distribution. (a), (b) Axion insulator phases with Dirac mass $M = 0.15$. (c), (d) Normal insulator phases with $M = -0.15$. The film thickness is taken as $n_z = 10$.

[Figs. 6(a) and 6(d)]. The electric field breaks the $\mathcal{PT}$ symmetry and causes energy offset between the degenerate bands [Figs. 6(b), 6(c), 6(e), and 6(f)].

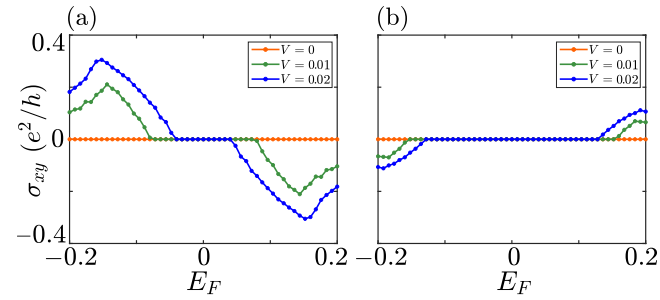

FIG. 8. Hall conductance calculated in the momentum space as functions of the Fermi energy E_F for different voltage V. (a) Axion insulator phases with Dirac mass $M = 0.15$. (b) Normal insulator phases with $M = -0.15$. The film thickness is $n_z = 10$.

Figure 7 shows the probability distribution of the bands in the normal insulator and axion insulators. In terms of the Berry curvature distributions in Fig. 6, we observe that it is the surface states that manifest the hidden layer Berry curvature in the two systems.

Figure 8 shows the Hall conductance of the axion insulator and normal insulator as functions of the Fermi energy E_F for different strength of the electric field. Here, the Hall conductance are calculated in the momentum space. The results are similar to the results shown in Figs. 3(a) and 3(e), except that the plateaus become smooth curves here.

[1] N. Nagaosa, J. Sinova, S. Onoda, A. H. MacDonald, and N. P. Ong, Anomalous Hall effect, Rev. Mod. Phys. **82**, 1539 (2010).

[2] J. Sinova, S. O. Valenzuela, J. Wunderlich, C. H. Back, and T. Jungwirth, Spin Hall effects, Rev. Mod. Phys. **87**, 1213 (2015).

[3] D. Xiao, W. Yao, and Q. Niu, Valley-contrasting physics in graphene: Magnetic moment and topological transport, Phys. Rev. Lett. **99**, 236809 (2007).

[4] W.-B. Dai, H. Li, D.-H. Xu, C.-Z. Chen, and X. C. Xie, Quantum anomalous layer Hall effect in the topological magnet $MnBi_2Te_4$, Phys. Rev. B **106**, 245425 (2022).

[5] A. Anirban, Quantum anomalous layer Hall effect, Nat. Rev. Phys. **5**, 271 (2023).

[6] A. Gao, Y.-F. Liu, C. Hu, J.-X. Qiu, C. Tzschaschel, B. Ghosh, S.-C. Ho, D. Berube, R. Chen, H. Sun *et al.*, Layer Hall effect in a 2D topological axion antiferromagnet, Nature (London) **595**, 521 (2021).

[7] R. Chen, H.-P. Sun, M. Gu, C.-B. Hua, Q. Liu, H.-Z. Lu, and X. C. Xie, Layer Hall effect induced by hidden Berry curvature in antiferromagnetic insulators, Natl. Sci. Rev. **11**, nwac140 (2022).

[8] C. Lei and A. H. MacDonald, Kerr, Faraday, and magnetoelectric effects in $MnBi_2Te_4$ thin films, Phys. Rev. B **108**, 125424 (2023).

[9] T. Zhang, X. Xu, B. Huang, Y. Dai, L. Kou, and Y. Ma, Layer-polarized anomalous Hall effects in valleytronic van der Waals bilayers, Mater. Horiz. **10**, 483 (2023).

[10] Y. Feng, Y. Dai, B. Huang, L. Kou, and Y. Ma, Layer Hall effect in multiferroic two-dimensional materials, Nano Lett. **23**, 5367 (2023).

[11] R.-L. Chu, J. Shi, and S.-Q. Shen, Surface edge state and half-quantized Hall conductance in topological insulators, Phys. Rev. B **84**, 085312 (2011).

[12] H. Zhou, H. Li, D.-H. Xu, C.-Z. Chen, Q.-F. Sun, and X. C. Xie, Transport theory of half-quantized Hall conductance in a semimagnetic topological insulator, Phys. Rev. Lett. **129**, 096601 (2022).

[13] J.-Y. Zou, B. Fu, H.-W. Wang, Z.-A. Hu, and S.-Q. Shen, Half-quantized Hall effect and power law decay of edge-current distribution, Phys. Rev. B **105**, L201106 (2022).

[14] P. A. Lee and T. V. Ramakrishnan, Disordered electronic systems, Rev. Mod. Phys. **57**, 287 (1985).

[15] F. Evers and A. D. Mirlin, Anderson transitions, Rev. Mod. Phys. **80**, 1355 (2008).

[16] C. W. J. Beenakker, Random-matrix theory of quantum transport, Rev. Mod. Phys. **69**, 731 (1997).

[17] D. Ma, A. Arora, G. Vignale, and J. C. W. Song, Anomalous skew-scattering nonlinear Hall effect and chiral photocurrents in $\mathcal{PT}$-symmetric antiferromagnets, Phys. Rev. Lett. **131**, 076601 (2023).

[18] R. B. Atencia, D. Xiao, and D. Culcer, Disorder in the nonlinear anomalous Hall effect of $\mathcal{PT}$-symmetric Dirac fermions, Phys. Rev. B **108**, L201115 (2023).

[19] N. A. Sinitsyn, Q. Niu, J. Sinova, and K. Nomura, Disorder effects in the anomalous Hall effect induced by Berry curvature, Phys. Rev. B **72**, 045346 (2005).

[20] I. A. Ado, I. A. Dmitriev, P. M. Ostrovsky, and M. Titov, Sensitivity of the anomalous Hall effect to disorder correlations, Phys. Rev. B **96**, 235148 (2017).

[21] O. Bleu, D. D. Solnyshkov, and G. Malpuech, Optical valley Hall effect based on transitional metal dichalcogenide cavity polaritons, Phys. Rev. B **96**, 165432 (2017).

[22] T. Olsen and I. Souza, Valley Hall effect in disordered monolayer MoS_2 from first principles, Phys. Rev. B **92**, 125146 (2015).

[23] C. Xu and J. E. Moore, Stability of the quantum spin Hall effect: Effects of interactions, disorder, and $\mathbb{Z}_2$ topology, Phys. Rev. B **73**, 045322 (2006).

[24] L. Sheng, D. N. Sheng, and C. S. Ting, Spin-Hall effect in two-dimensional electron systems with Rashba spin-orbit coupling and disorder, Phys. Rev. Lett. **94**, 016602 (2005).

[25] B. Huckestein, Scaling theory of the integer quantum Hall effect, Rev. Mod. Phys. **67**, 357 (1995).

[26] S. A. Trugman, Localization, percolation, and the quantum Hall effect, Phys. Rev. B **27**, 7539 (1983).

[27] J. Li, R.-L. Chu, J. K. Jain, and S.-Q. Shen, Topological Anderson insulator, Phys. Rev. Lett. **102**, 136806 (2009).

[28] B. Wu, J. Song, J. Zhou, and H. Jiang, Disorder effects in topological states: Brief review of the recent developments, Chin. Phys. B **25**, 117311 (2016).

[29] E. J. Meier, F. A. An, A. Dauphin, M. Maffei, P. Massignan, T. L. Hughes, and B. Gadway, Observation of the topological Anderson insulator in disordered atomic wires, Science **362**, 929 (2018).

[30] S. Stützer, Y. Plotnik, Y. Lumer, P. Titum, N. H. Lindner, M. Segev, M. C. Rechtsman, and A. Szameit, Photonic topological Anderson insulators, Nature (London) **560**, 461 (2018).

[31] G.-G. Liu, Y. Yang, X. Ren, H. Xue, X. Lin, Y.-H. Hu, H.-X. Sun, B. Peng, P. Zhou, Y.-Chong *et al.*, Topological Anderson insulator in disordered photonic crystals, Phys. Rev. Lett. **125**, 133603 (2020).

[32] X. Cui, R.-Y. Zhang, Z.-Q. Zhang, and C. T. Chan, Photonic $\mathbb{Z}_2$ topological Anderson insulators, Phys. Rev. Lett. **129**, 043902 (2022).

[33] X. Li, H. Xu, J. Wang, L.-Z. Tang, D.-W. Zhang, C. Yang, T. Su, C. Wang, Z. Mi, W. Sun *et al.*, Mapping a topology-disorder phase diagram with a quantum simulator, arXiv:2301.12138.

[34] H. Liu, B. Xie, H. Wang, W. Liu, Z. Li, H. Cheng, J. Tian, Z. Liu, and S. Chen, Acoustic spin-Chern topological Anderson insulators, Phys. Rev. B **108**, L161410 (2023).

[35] C.-X. Liu, X.-L. Qi, H. J. Zhang, X. Dai, Z. Fang, and S.-C. Zhang, Model Hamiltonian for topological insulators, Phys. Rev. B **82**, 045122 (2010).

[36] H. Zhang, C.-X. Liu, X.-L. Qi, X. Dai, Z. Fang, and S.-C. Zhang, Topological insulators in Bi_2Se_3, Bi_2Te_3, and Sb_2Te_3 with a single Dirac cone on the surface, Nat. Phys. **5**, 438 (2009).

[37] J.-X. Qiu, C. Tzschaschel, J. Ahn, A. Gao, H. Li, X.-Y. Zhang, B. Ghosh, C. Hu, Y.-X. Wang, Y.-F. Liu *et al.*, Axion optical induction of antiferromagnetic order, Nat. Mater. **22**, 583 (2023).

[38] T. Morimoto, A. Furusaki, and N. Nagaosa, Topological magnetoelectric effects in thin films of topological insulators, Phys. Rev. B **92**, 085113 (2015).

[39] J. Wang, B. Lian, X.-L. Qi, and S.-C. Zhang, Quantized topological magnetoelectric effect of the zero-plateau quantum anomalous Hall state, Phys. Rev. B **92**, 081107(R) (2015).

[40] K. Nomura and N. Nagaosa, Surface-quantized anomalous Hall current and the magnetoelectric effect in magnetically disordered topological insulators, Phys. Rev. Lett. **106**, 166802 (2011).

[41] X.-L. Qi and S.-C. Zhang, Topological insulators and superconductors, Rev. Mod. Phys. **83**, 1057 (2011).

[42] X.-L. Qi, T. L. Hughes, and S.-C. Zhang, Topological field theory of time-reversal invariant insulators, Phys. Rev. B **78**, 195424 (2008).

[43] J. Yu, J. Zang, and C.-X. Liu, Magnetic resonance induced pseudoelectric field and giant current response in axion insulators, Phys. Rev. B **100**, 075303 (2019).

[44] D. Xiao, J. Jiang, J.-H. Shin, W. Wang, F. Wang, Y.-F. Zhao, C. Liu, W. Wu, M. Chan, N. Samarth *et al.*, Realization of the axion insulator state in quantum anomalous Hall sandwich heterostructures, Phys. Rev. Lett. **120**, 056801 (2018).

[45] M. Mogi, M. Kawamura, R. Yoshimi, A. Tsukazaki, Y. Kozuka, N. Shirakawa, K. S. Takahashi, M. Kawasaki, and Y. Tokura, A magnetic heterostructure of topological insulators as a candidate for an axion insulator, Nat. Mater. **16**, 516 (2017).

[46] C.-X. Liu, H. Zhang, B. Yan, X.-L. Qi, T. Frauenheim, X. Dai, Z. Fang, and S.-C. Zhang, Oscillatory crossover from two-dimensional to three-dimensional topological insulators, Phys. Rev. B **81**, 041307(R) (2010).

[47] W.-Y. Shan, H.-Z. Lu, and S.-Q. Shen, Effective continuous model for surface states and thin films of three-dimensional topological insulators, New J. Phys. **12**, 043048 (2010).

[48] Y. Zhang, K. He, C.-Z. Chang, C.-L. Song, L.-L. Wang, X. Chen, J.-F. Jia, Z. Fang, X. Dai, W.-Y. Shan *et al.*, Crossover of the three-dimensional topological insulator Bi_2Se_3 to the two-dimensional limit, Nat. Phys. **6**, 584 (2010).

[49] J. Linder, T. Yokoyama, and A. Sudbø, Anomalous finite size effects on surface states in the topological insulator Bi_2Se_3, Phys. Rev. B **80**, 205401 (2009).

[50] H.-P. Sun, C. M. Wang, S.-B. Zhang, R. Chen, Y. Zhao, C. Liu, Q. Liu, C. Chen, H.-Z. Lu, and X. C. Xie, Analytical solution for the surface states of the antiferromagnetic topological insulator $MnBi_2Te_4$, Phys. Rev. B **102**, 241406(R) (2020).

[51] Y. Li, C. Liu, Y. Wang, Z. Lian, S. Li, H. Li, Y. Wu, H.-Z. Lu, J. Zhang, and Y. Wang, Giant nonlocal edge conduction in the axion insulator state of $MnBi_2Te_4$, Sci. Bull. **68**, 1252 (2023).

[52] C. Liu, Y. Wang, H. Li, Y. Wu, Y. Li, J. Li, K. He, Y. Xu, J. Zhang, and Y. Wang, Robust axion insulator and Chern insulator phases in a two-dimensional antiferromagnetic topological insulator, Nat. Mater. **19**, 522 (2020).

[53] M. Mogi, M. Kawamura, A. Tsukazaki, R. Yoshimi, K. S. Takahashi, M. Kawasaki, and Y. Tokura, Tailoring tricolor structure of magnetic topological insulator for robust axion insulator, Sci. Adv. **3**, eaao1669 (2017).

[54] Y. Tokura, K. Yasuda, and A. Tsukazaki, Magnetic topological insulators, Nat. Rev. Phys. **1**, 126 (2019).

[55] C. W. Groth, M. Wimmer, A. R. Akhmerov, J. Tworzydło, and C. W. J. Beenakker, Theory of the topological Anderson insulator, Phys. Rev. Lett. **103**, 196805 (2009).

[56] R. S. K. Mong, A. M. Essin, and J. E. Moore, Antiferromagnetic topological insulators, Phys. Rev. B **81**, 245209 (2010).

[57] A. M. Essin, J. E. Moore, and D. Vanderbilt, Magnetoelectric polarizability and axion electrodynamics

in crystalline insulators, Phys. Rev. Lett. **102**, 146805 (2009).

[58] B. Fu, Z.-A. Hu, and S.-Q. Shen, Bulk-hinge correspondence and three-dimensional quantum anomalous Hall effect in second-order topological insulators, Phys. Rev. Res. **3**, 033177 (2021).

[59] E. Prodan, Disordered topological insulators: a non-commutative geometry perspective, J. Phys. A: Math. Theor. **44**, 113001 (2011).

[60] E. Prodan, Robustness of the spin-Chern number, Phys. Rev. B **80**, 125327 (2009).

[61] J. Cao, W. Jiang, X.-P. Li, D. Tu, J. Zhou, J. Zhou, and Y. Yao, In-plane anomalous Hall effect in $\mathcal{PT}$-symmetric antiferromagnetic materials, Phys. Rev. Lett. **130**, 166702 (2023).

[62] C.-K. Chiu, J. C. Y. Teo, A. P. Schnyder, and S. Ryu, Classification of topological quantum matter with symmetries, Rev. Mod. Phys. **88**, 035005 (2016).